# A comparative study of the gas-particle partitioning of PCDD/Fs, PCBs, and PAHs

**ARTICLE** *in* ENVIRONMENTAL SCIENCE AND TECHNOLOGY · OCTOBER 2000

Impact Factor: 5.33 · DOI: 10.1021/es9913232



**4 AUTHORS**, INCLUDING:

Rainer Lohmann
University of Rhode Island
**112** PUBLICATIONS **3,813** CITATIONS
SEE PROFILE

Tom Harner
Environment Canada
**203** PUBLICATIONS **11,368** CITATIONS
SEE PROFILE

Kevin C Jones
Lancaster University
**668** PUBLICATIONS **29,206** CITATIONS
SEE PROFILE

*Environ. Sci. Technol.* **2000**, *34,* 4943−4951

# A Comparative Study of the Gas-Particle Partitioning of PCDD/Fs, PCBs, and PAHs

RAINER LOHMANN,*,‡ TOM HARNER,§ GARETH O. THOMAS, AND KEVIN C. JONES

*Department of Environmental Science, IENS, Lancaster University, Lancaster, LA1 4YQ, U.K.*

Air samples were taken concurrently for four sampling events in the winter of 1998 at three contrasting sites: an urban center and two rural sites. The rural sites were characterized by the extensive usage of coal and wood for space heating. Samples were analyzed for PCDD/Fs, PCBs, and PAHs. Recently measured octanol−air partition coefficients ($K_{oa}$) for PCDD/Fs enabled a comparison of the $K_{oa}$-based versus the subcooled liquid vapor pressure ($p_L$)-based partition model for all three compound classes. Both $K_{oa}$ and $p_L$ were found to be excellent descriptors of the gas-particle partitioning of PCDD/Fs, PCBs, and PAHs. However, regressions for log $K_p$-log $p_L$ gave higher regression coefficients than for log $K_p$-log $K_{oa}$. Both models showed roughly similar relative states of equilibrium for PCDD/Fs, PCBs, and PAHs. PCBs were closest to equilibrium at the urban site. It is argued that newly released particles at the rural sites caused nonequilibrium partitioning at those sites for PCBs. PAHs were released at all sites and were, in line with expectations, approaching equilibrium. The $K_{oa}$-based and the $p_L$-based model gave contradictory results for PCDD/Fs: according to the $p_L$-model, PCDD/Fs were in equilibrium for event I but not for the other events, whereas the $K_{oa}$-model showed the PCDD/Fs not being in equilibrium for event I. A simple $K_{oa}$-model, combining advective transport and locally released PCDD/Fs and PAHs, can explain the observed nonequilibrium partitioning for the first sampling event.

## Introduction

Atmospheric transport is key to moving most persistent organic pollutants (POPs) from sources to remote regions and in contaminating terrestrial and aquatic environments and the food chain. The atmospheric fate of POPs is primarily governed by their gas-particle partitioning. Wet (wash- and rainout) and dry deposition, photolysis, and reaction with OH radicals act differently on gas- and particle-bound semivolatile organic compounds (SVOCs), thereby affecting the efficiency and scope of their long-range atmospheric transport (*1*). The partitioning of a given compound between the particulate and the gas phase depends on the ambient temperature, the nature of ambient aerosols, and interactions between the compound and the aerosol (e.g. refs *2* and *3*).

Two different sorption models have been used to describe the partitioning of SVOCs, namely adsorption onto the particle surface and, more recently, absorption into the organic phase of aerosols (*2*−*8*). Absorptive partitioning is believed to be the dominant mechanism when an organic fraction exists on the aerosol (*2, 9*). The subcooled liquid vapor pressure ($p_L$) has been used to describe both adsorptive and absorptive partitioning (*2*). Absorptive partitioning has also been successfully described using the octanol−air partition coefficient ($K_{oa}$) (*5, 6*). Values of $K_{oa}$ have been measured for polychlorinated biphenyls (PCBs) (*10*−*12*), polychlorinated naphthalenes (PCNs), polycyclic aromatic hydrocarbons (PAHs) (*13*), and polychlorinated dibenzo-*p*-dioxins and dibenzofurans (PCDD/Fs) (*14*).

This paper describes an investigation of the concurrent partitioning of three classes of POPs, namely PCDD/Fs, PCBs, and PAHs. Important differences exist in the manner in which these compound classes enter the atmosphere and become available for gas-particle exchange. For instance PCDD/Fs and PAHs are released as emissions from combustion and industrial processes and consequently may already be associated with particulate matter. PCBs are introduced primarily by volatilization from in-use and disposed electrical and hydraulic equipment or as re-emissions from soil (*15*) and thus partition to the "exchangeable fraction" of the already formed aerosol. The properties of the aerosol will also differ depending on their transport time ("ageing") and their origin/formation process, e.g. high versus low-temperature (wood stove and diesel generated) combustion aerosols (*16, 17*). This too will affect partitioning. Each compound class covers a wide range of $p_L$- (Pa) and log $K_{oa}$-values: ($10^{-2}$−$10^{-7}$) Pa and 8−12 for PCDD/Fs; ($10^{-1}$−$10^{-4}$) Pa and 7−11 for PCBs, and ($10^{+1}$−$10^{-6}$) Pa and 6−12 for PAHs, respectively. There are very few comparative studies of different POPs classes (e.g. refs *18*−*20*), rarely involving PCDD/Fs.

In this study, we compared the partitioning of PCDD/Fs, PAHs, and PCBs at different locations in northern England in the winter of 1998. The aim was to better understand the importance of source types, the proximity to sources, and the influence of meteorology on the gas-particle distributions of these important compound classes. For the first time measured $K_{oa}$-values are available for PCDD/Fs which allows us to compare $K_{oa}$-based versus $p_L$-based models of gas-particle partitioning.

## Materials and Methods

**Sampling Locations**. The study sites were chosen to encompass a range of aerosol types and potential sources of POPs. They were (Figure 1) as follows: (i) Manchester, an urban center, comprising ∼3 million inhabitants with traffic and heavy industries (site A) and (ii and iii) Clapham and Austwick, small villages in the Yorkshire Dales National Park (sites B and C) with a strong impact of domestic burning. The site A sampler was located on the top of the High Court, ca. 25 m above ground level, close to the town center. It is ∼100 km south of the other sites. The two rural sites, Clapham (site B) and Austwick (site C), are ∼50 km east of Lancaster. Both villages have ∼200 households (1991 census data) and are located at the slopes of Ingleborough (720 m high), a hill in the Yorkshire Dales National Park. At both sites, domestic burning of coal and wood is extensive during the winter months, because there is no natural gas supplied to the villages. Samplers were installed at ground-level.

* Corresponding author phone: (617)258-6835; fax: (617)253-7475; e-mail: lohmannr@mit.edu.

‡ Present address: Ralph M. Parsons Laboratory, Department of Civil and Environmental Engineering, Massachusetts Institute of Technology, 48-336, Cambridge, MA 02139.

§ Present address: Atmospheric Environment Service, Environment Canada, 4905 Dufferin Street, Downsview, Ontario M3H 5T4, Canada.

10.1021/es9913232 CCC: $19.00 
Published on Web 10/27/2000

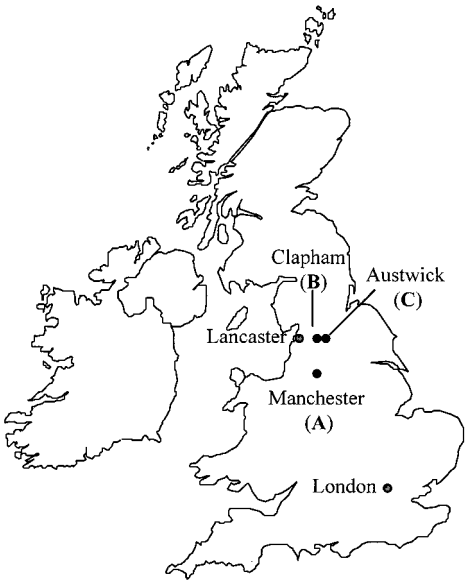


**FIGURE 1. Map of the sampling sites in northwest England in the U.K.**

**Air Sampling**. Four high volume (hi-vol) air samples were collected concurrently for 72−96 h at all three sites in February 1998. The sampling dates and volumes, total suspended particulate matter concentrations (TSP), air mass origins, and meteorological parameters are given in Table 1. Air samples were taken with GPS-1 air samplers (Graseby Andersen) equipped with a Whatman glass fiber filter (GFF, 10 cm diameter) for collecting particle-bound compounds and two polyurethane foam plugs (PUF, 5 cm diameter, 6.25 cm length) in series for retaining compounds in the gaseous phase (for more details see ref *21*). The GFFs were equilibrated in a humidity controlled atmosphere 24 h before and after sampling and weighed to obtain TSP concentrations. More details on the sampling procedure can be found in ref *21*.

**Analytical Procedures**. The analytical methods employed have been described elsewhere (PCDD/Fs (*22*); PCB-23; PAHs-24) and are summarized in ref *21*. Target compounds were chosen that were readily detectable in the particle and gas phases and cover a wide range of particle-phase distributions. They included the following: $Cl_{2-6}$DD/Fs, the 2,3,7,8-substituted $Cl_{4-6}$DFs and $Cl_{4-5}$DDs, coplanar PCBs 126 and 169, PCBs 31, 60, 61/74, 66, 101, 118, 138, 153, 180, 183, 187, and the PAHs phenanthrene (Phen), anthracene (An), 1-methylphenanthrene (1-MePh), fluoranthene (FA), pyrene (Pyr), benzo[*a*]anthracene (BaA), chrysene/triphenylene (Chr/Tri), benzo[*b*]fluoranthene (BbFA), and benzo[*k*]fluoranthene (BkFA).

**Quality Control.** For every nine samples, a field blank, a laboratory blank, and a reference soil were incorporated in the analytical procedure. Detection limits (d.l.) were derived from the blanks and quantified as three times the standard deviation of the mean concentration in the blanks. When 2,3,7,8-substituted PCDD/Fs were not detected, the noise of the baseline plus three times its standard deviation was taken as the detection limit. Average field blank concentrations, higher than the laboratory blanks, were subtracted from the samples. Mean recoveries for the $^{13}C_{12}$-2,3,7,8-substituted CDD/Fs were 44−122% and 31−79% for $^{13}C_{12}$−$Cl_{2/3}$DD/Fs; 29−94% for the $^{13}C_{12}$ coplanar PCBs; between 24 and 115% for $^{13}C_{12}$−PCBs; and 42−157% for the deuterated PAHs. Based on air volumes of 800 $m^3$, detection limits (fg/$m^3$) were 0.1−0.5 for the 2,3,7,8-substituted $Cl_{4-6}$DD/Fs, 13 for $Cl_2$DDs, 55 for $Cl_2$DFs, and ≤5 for $Cl_{3-6}$DD/Fs; ≤1 fg/$m^3$ for PCBs #126 and #169; ∼2 pg/$m^3$ for PCB # 31 and ∼0.5 pg/$m^3$ for the other PCBs; ∼1.5 ng/$m^3$ for An, Phen, Pyr; and <1 ng/$m^3$ for the other PAHs. Average blank concentrations (fg/$m^3$) were ∼35 for $Cl_2$DFs, 7 for $Cl_2$DDs, and ≤2 for $Cl_{3-6}$DD/Fs; ≤1 fg/$m^3$ for PCBs #126 and #169; <1 pg/$m^3$ for PCB 31 and <0.3 pg/$m^3$ for the other PCBs; ∼2 ng/$m^3$ for Phen; and ∼1 ng/$m^3$ for the other PAHs.

**Sampling Artifacts**. For hi-vol air sampling, gas and particulate phases are operationally defined: the compounds retained by the GFF as "particulate-bound" and compounds trapped by the PUF as gas phase. Known hi-vol sampling artifacts include the following: (i) particle blow-off from the GFF, (ii) adsorption to the GFF, (iii) "stripping" of compounds from the particle phase onto the PUF, and (iv) breakthrough of compounds in the absorbent. Based on experiments carried out in our laboratory we did not consider adsorption to a back-up GFF or loss of gaseous compounds through both PUFs as being significant (e.g. ref *25*). Pankow and Bidleman (*4*) noted that changes in the analytes' ambient air concentration and/or temperature (*T*) during the sampling period may lead to adsorption/desorption of particulate-bound analytes and result in a measured particle-gas distribution that is not in equilibrium. Although this artifact could not be eliminated from this study we expect it to be of minor significance since *T* ranges for the sampling events were usually < 10 °C (see Table 1).

**Subcooled Liquid Vapor Pressures ($p_L$).** PCDD/F-$p_L$-values were taken from Eitzer and Hites (*26*), with retention time indices from Donelly et al. (*27*) and Hale et al. (*28*). The $p_L$-values were *T*-corrected based on the variation of $p_L$ with *T* as reported by Eitzer and Hites (*26*). PCDD/F homologue group vapor pressures were calculated by averaging the available congener specific data for each homologue group. *T*-dependent $p_L$-values for PAHs were taken from Yamasaki et al. (*29*); missing $p_L$ were obtained from correlation with molecular weight (*M*; $r^2 = 0.99$) for each *T*. Falconer and Bidleman's *T*-dependent $p_L$-values were used for PCBs (*30*).

Octanol−air partition coefficients ($K_{oa}$): Dimensionless $K_{oa}$-values for PAHs were calculated at a *T* of 298 K according to

$$K_{oa} = K_{ow}RT/H \quad (1)$$

where $K_{ow}$ is the octanol−water partition coefficient, *H* is the Henry's Law constant, and *R* is the universal gas constant. Missing $K_{oa}$-values were obtained from the correlation of the thus calculated $K_{oa}$-values with *M* ($r^2 = 0.96$ (*31*)). PAH−$K_{oa}$ were *T*-corrected based on work by Harner and Bidleman using the regression of calculated versus measured $K_{oa}$-values ($r^2 = 0.99$) at each sampling *T* (*13*). *T*-dependent $K_{oa}$-values for PCBs were taken from Harner and Bidleman (*11*) and for PCDD/Fs from Harner et al. (*14*).

## Results and Discussion

**Air Concentrations of PCDD/Fs, PAHs, and PCBs**. Ambient air concentrations of PCDD/Fs, PAHs, and PCBs varied widely over the four sampling events (see Table 2): highest concentrations of $\Sigma Cl_{4-8}$DD/Fs and ΣPAHs were observed on event I. Later concentrations were factors of 3−8 lower for PCDD/Fs and decreased by factors of 2−4 for PAHs (see Table 2). PCBs did not exhibit this trend of elevated concentrations during the first sampling event. We should note, however, that at the Manchester site (A), ΣPCB levels increased with increasing *T* from 370 (event I, ∼2 °C) to 720 pg/$m^3$ (event IV, ∼12 °C). At sites B and C, ΣPCB levels were generally low, at ∼50−85 pg/$m^3$, and were not correlated with *T*. In general the observed air concentrations of PCDD/Fs, PCBs, and PAHs were typical for winter samples at urban and rural locations in the U.K. (*32*−*35*). The only exception were ΣPAHs at Austwick (site C) where air concentrations were more typical of urban air.

**TABLE 1. Sampling Dates, Air Volumes ($m^3$), TSP-Concentrations ($\mu g/m^3$), Average (Minimum and Maximum) Temperature (°C), and Rainfall (mm) for the Individual Sample Numbers and Dates**

| | | dates | | | |
|---|---|---|---|---|---|
| | | event I (30.1.– 3.2.98) | event II (3.– 6.2.98) | event III (6.–10.2.98) | event IV (10.– 13.2.98) |
| sites | air mass origin | NW (UK) | W/SW (Ireland) | SW/W | SW |
| A (Manchester) | air volume | 703 | 649 | 953 | 733 |
| | TSP | 57 | 54[a] | 44 | 61 |
| | $T^b$ ($T_{min}$-$T_{max}$) | 2.4 (−4.0–8.0) | 5.7 (0.0–11.0) | 7.6 (2.0–11.0) | 11.8 (9.0–15.0) |
| | rain | 0.4 | 5.3 | 1.0 | 0.1 |
| B (Clapham) | air volume | 609 | 698 | 882 | 717 |
| | TSP | 65 | 36[a] | 36[a] | 38 |
| | $T^b$ ($T_{min}$-$T_{max}$) | 2.7 (−1.5–7.0) | 3.8 (0.0–5.9) | 4.3 (−0.5–7.8) | 8.3 (5.5–10.6) |
| | rain | 0.7 | 1.6 | 6.9 | 4.7 |
| C (Austwick) | air volume | 743 | 616 | 788 | 714 |
| | TSP | 45 | 54 | 26 | 40[a] |
| | $T^b$ ($T_{min}$-$T_{max}$) | 2.7 (−1.5–7.0) | 3.8 (0.0–5.9) | 4.3 (−0.5–7.8) | 8.3 (5.5–10.6) |
| | rain | 0.7 | 1.6 | 6.9 | 4.7 |

[a] TSP estimated based on average TSP concentrations at the site. [b] Calculated as the average of $T_{min}$ and $T_{max}$ throughout the sampling period.

**TABLE 2. $\Sigma Cl_{4-8}$DD/Fs ($pg/m^3$), PCDD/F-ΣTEQ[a] ($fg/m^3$), ΣPCBs ($pg/m^3$), and ΣPAHs ($ng/m^3$) for the Different Sampling Events at the Three Sites**

| sites | | event I | event II | event III | event IV |
|---|---|---|---|---|---|
| A | $\Sigma Cl_{4-8}$DD/Fs | 17 | 4.8 | 2.6 | 2.1 |
| | ΣTEQ[a] | 220 | 64 | 37 | 26 |
| | ΣPCBs | 370 | 420 | 570 | 720 |
| | ΣPAHs | 120 | 59 | 30 | 37 |
| B | $\Sigma Cl_{4-8}$DD/Fs | 4.8 | 0.99 | 0.88 | 0.82 |
| | ΣTEQ[a] | 64 | 11 | 14 | 14 |
| | ΣPCBs | 85 | 53 | 51 | 69 |
| | ΣPAHs | 110 | 17 | 28 | 16 |
| C | $\Sigma Cl_{4-8}$DD/Fs | 3.6 | 1.1 | 1.1 | 0.80 |
| | ΣTEQ[a] | 52 | 13 | 18 | 11 |
| | ΣPCBs | 68 | 60 | 68 | 84 |
| | ΣPAHs | 96 | 46 | 65 | 37 |

[a] Reference *36*.

In a related study (*21*), air samples were collected at sites A, B, and C in the winter of 1998 to assess the contribution of local sources to the ambient air concentrations of PCDD/Fs, PCBs, and PAHs. Findings showed that local sources at the villages (sites B and C) accounted for ~25% of the PCDD/F-ΣTEQ (WHO-TEFs (*36*)) and ~75% of the ΣPAHs. This was mostly attributed to local domestic burning. No site-specific PCB signal was found. Urban site A was found to be a source area for all three POPs classes studied (*21*).

**Overview of Measured Gas-Particle Distributions**. The wide spectrum of volatilities for the compound classes studied resulted in substantial differences in partitioning behavior. The $Cl_{2-3}$DD/Fs were mostly in the gas phase, with 0–30% bound to particles. $Cl_6$DD/Fs were 69–100% associated with the particulate phase. $Cl_{4/5}$DD/Fs varied markedly between the two phases, from 7 to 98% particle-bound, depending on *T*, TSP, and sampling event. PCBs were >50% in the gas phase at sites B and C, with the exception of congener 180 (21–80%). At site A, for the coldest event (I), PCBs 138, 153, 183, and 187 were also >50% particulate-bound. PAHs up to a *M* of 202 (Pyr) were generally <25% associated with particles,while PAHs with $M \geq 252$ were predominantly in the particulate phase. A more detailed analysis of the results of this study will follow that will consider both $p_L$- and $K_{oa}$-based models of partitioning.

**Junge–Pankow Model.** An adsorptive partitioning model, based on work by Junge (*37*) and Pankow (*38*), has often been used to predict the gas-particle distribution of SVOCs

$$\phi = c\theta/(p_L^\circ + c\theta) \quad (2)$$

where $\phi$ is the particulate-bound fraction, $\theta$ is the particle surface area per volume of air, and *c* is a constant which depends on the heat of condensation of the chemical and surface properties. $\theta$-values often used in the literature are $4.2 \times 10^{-5}$ (clean continental background), $1.5 \times 10^{-4}$ (rural conditions), and $1.1 \times 10^{-3}$ $m^2/m^3$ (urban) (e.g. refs *6* and *37*). Junge assumed a value of $c = 0.172$ Pa m; this value has been used frequently and was also employed in this study. However, it is uncertain if the value is appropriate.

For most samples (see Figure 2a for event II, site A, Manchester) the measured PCDD/F partitioning did not follow any one theoretical curve; rather, the higher chlorinated congeners (log $p_L$ < -4.5) were closer to the urban partitioning curve, while the lower chlorinated congeners (log $p_L$ > -4.5) were closer to the rural curve. The PCB data were closer to the rural curve for site A; for the other sites the degree of scatter for PCBs was greater, and the data were closer to the clean background partitioning curve. Gas-particle distribution of individual PAHs were on both sides of the rural partitioning curve.

The distribution of a chemical between the gas and particulate phase is usually defined using the particle-gas partition coefficient, $K_P$

$$K_p = (F/A)/\mathrm{TSP} \quad (3)$$

where *F* and *A* are the analyte concentrations on the GFF and on the PUF, respectively, and TSP is in $\mu g/m^3$ (*39*). Only data points where the analytes were above the detection limit in both phases were included in the calculations. When log $K_p$ is regressed against the *T*-corrected log $p_L$ of the compound (eq 4), useful information about the partitioning can be extracted from the slope, $m_r$, and the *y*-intercept, $b_r$, of the trendline (*39*):

$$\log K_p = m_r \log p_L + b_r \quad (4)$$

For equilibrium partitioning of the chemical between the gas and particulate phase a slope of $m_r$ near −1 is expected (*3*). However, Goss and Schwarzenbach (*9*) and Simcik et al. (*18*) argue that deviations from $m_r = -1$ are not always indicative of disequilibrium. The intercept $b_r$ is dependent on properties associated with the aerosol. For adsorptive partitioning $b_r$ is related to the number of adsorption sites on the particle surface and surface-chemical interactions

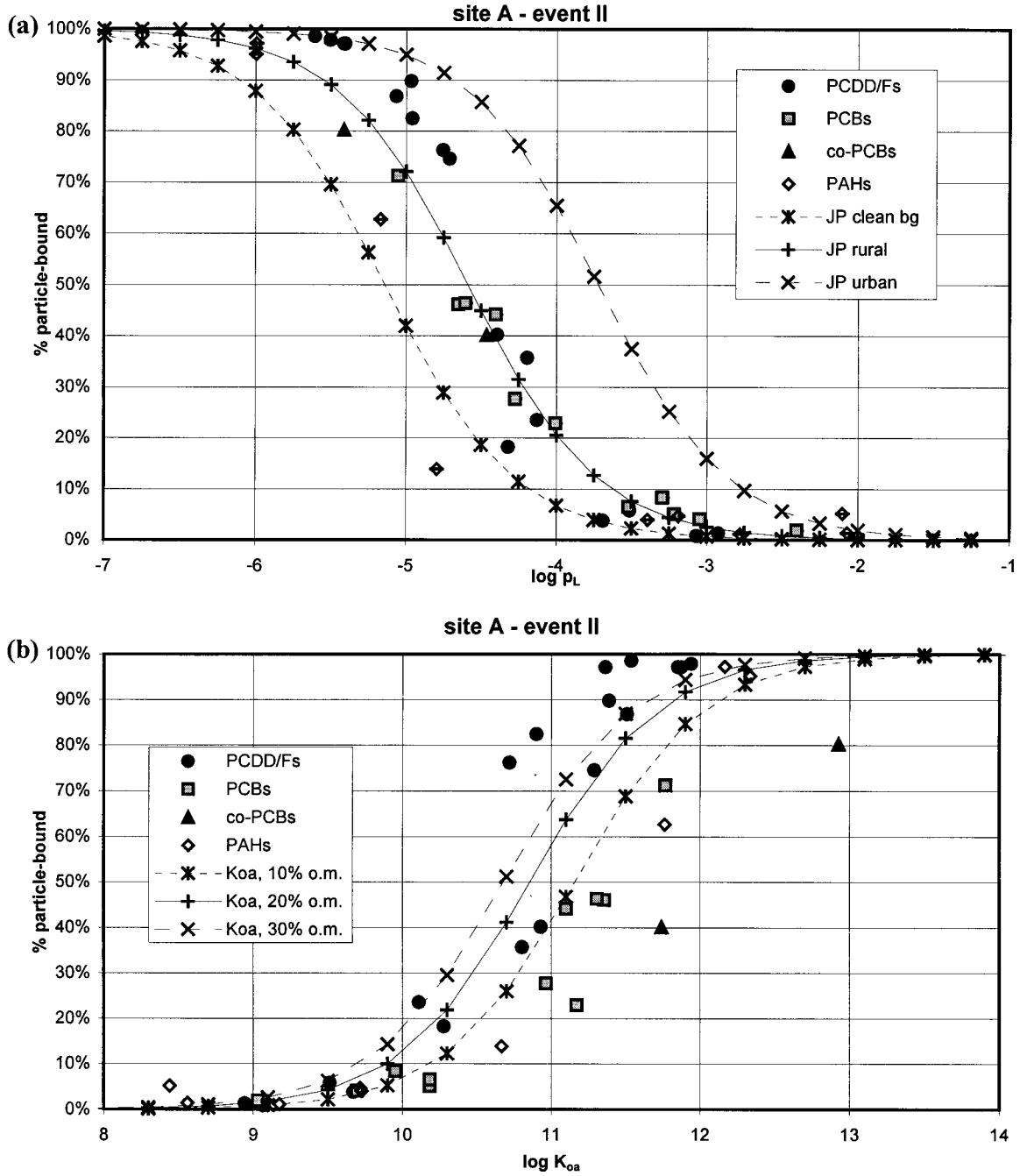


**FIGURE 2. (a) Junge-Pankow and (b) $K_{oa}$ plots with measured data for site A for event II.**

(*3*). For absorptive partitioning $b_r$ is associated with the capacity of the absorbing matrix for accommodating the chemical; more specifically, to the fraction of organic matter on the particle surface and the activity coefficient of the absorbing compound in the organic matter (*3*).

Correlations of log $K_p$ versus log $p_L$ were in general highly significant (at $P \leq 0.01$) for PCDD/Fs, PCBs, and PAHs (see Table 3). Log $K_p$ − log $p_L$ plots for site A are shown in Figure 3; those for sites B and C can be found in the Supporting Information as Figures 1S and 2S.

***$K_{oa}$* Absorption**. Finizio et al. (*5*) and Harner and Bidleman (*6*) showed that $K_{oa}$ is a useful descriptor of absorptive partitioning of chemicals into the organic matrix of aerosols. The Junge−Pankow model is parametrized using $K_{oa}$ to give the following relation

$$\log K_p = m_r \log K_{oa} + \log f_{om} - 11.91 \qquad (5)$$

where $f_{om}$ is the fraction of organic matter (om) in the aerosol. For equilibrium partitioning $m_r$ is expected to have a value of near +1. The intercept depends on the value of $f_{om}$ which determines the absorptive capacity of the aerosol, i.e., $b_r = \log f_{om} - 11.91$. The predicted particulate fraction $\phi$ is calculated as

$$\phi = K_p\text{TSP}/(K_p\text{TSP} + 1) \qquad (6)$$

Figure 2b shows the measured (event II, site A) and predicted (eq 6) particulate fractions based on aerosols consisting of 10, 20, and 30% om. The lower chlorinated PCDD/Fs ($\log K_{oa} \leq 10.5$) were in general close to the partitioning predicted by 20−30% om in the aerosols, while the higher chlorinated PCDD/Fs ($\log K_{oa} \geq 10.5$) often showed higher particle phases than predicted by 30% om. PCBs showed a higher degree of scatter and had lower particle-bound fractions than predicted

**TABLE 3. Correlations of Logarithm $K_p$ versus Logarithm $p_L$ for 12 Samples with the Square of Pearson's Product Moment Correlation Coefficient ($r^2$), the Number of Datapoints Used ($n$), and the Slope ($m_r$) and Intercept ($b_r$) of the Trendline**

| $p_L$ sites | | PCDD/Fs I | PCDD/Fs II | PCDD/Fs III | PCDD/Fs IV | PCBs I | PCBs II | PCBs III | PCBs IV | PAHs I | PAHs II | PAHs III | PAHs IV |
|---|---|---|---|---|---|---|---|---|---|---|---|---|---|
| A | $r^2$ | 0.95[a] | 0.98[a] | 0.95[a] | 0.95[a] | 0.96[a] | 0.98[a] | 0.57[a] | 0.74[a] | 0.96[a] | 0.85[a] | 0.77[a] | 0.94[b] |
| | ($n$) | (18) | (18) | (16) | (15) | (13) | (13) | (13) | (13) | (9) | (9) | (8) | (4) |
| | $m_r$ | −1.1 | −1.5 | −1.3 | −1.3 | −0.77 | −0.80 | −0.35 | −0.62 | −0.72 | −0.77 | −0.64 | −0.62 |
| | $b_r$ | −6.5 | −8.4 | −7.7 | −7.3 | −5.1 | −5.5 | −3.8 | −5.4 | −5.2 | −5.4 | −4.8 | −5.1 |
| B | $r^2$ | 0.96[a] | 0.97[a] | 0.98[a] | 0.97[a] | 0.64[a] | 0.68[a] | 0.75[b] | 0.75[a] | 0.91[a] | 0.73[b] | 0.93[a] | 0.82[a] |
| | ($n$) | (13) | (15) | (15) | (13) | (13) | (11) | (7) | (13) | (8) | (7) | (9) | (9) |
| | $m_r$ | −1.3 | −1.3 | −1.2 | −1.3 | −0.59 | −0.22 | −0.48 | −0.47 | −0.81 | −0.58 | −0.75 | −0.65 |
| | $b_r$ | −6.9 | −7.6 | −7.0 | −7.3 | −4.5 | −3.1 | −4.2 | −4.1 | −5.6 | −4.4 | −5.0 | −4.9 |
| C | $r^2$ | 0.90[a] | 0.88[a] | 0.98[a] | 0.91[a] | 0.84[a] | 0.65[a] | 0.70[a] | 0.74[a] | 0.97[a] | 0.87[a] | 0.98[a] | 0.90[a] |
| | ($n$) | (18) | (17) | (17) | (15) | (9) | (11) | (9) | (9) | (9) | (7) | (9) | (6) |
| | $m_r$ | −0.89 | −1.1 | −1.2 | −1.1 | −0.87 | −0.26 | −0.47 | −0.49 | −0.79 | −0.74 | −0.87 | −0.71 |
| | $b_r$ | −5.4 | −6.7 | −6.9 | −6.7 | −5.9 | −3.6 | −4.2 | −4.5 | −5.3 | −4.9 | −5.4 | −5.2 |

[a] Significant at $P \leq 0.01$. [b] Significant at $P \leq 0.05$.

**TABLE 4. Correlations of Logarithm $K_p$ versus Logarithm $K_{oa}$ for 12 Samples with the Square of Pearson's Product Moment Correlation Coefficient ($r^2$) and the Slope ($m_r$) and Intercept ($b_r$) of the Trendline**

| $K_{oa}$ sites | | PCDD/Fs I | PCDD/Fs II | PCDD/Fs III | PCDD/Fs IV | PCBs I | PCBs II | PCBs III | PCBs IV | PAHs I | PAHs II | PAHs III | PAHs IV |
|---|---|---|---|---|---|---|---|---|---|---|---|---|---|
| A | $r^2$ | 0.90[a] | 0.92[a] | 0.89[a] | 0.92[a] | 0.95[a] | 0.91[a] | 0.62[a] | 0.80[a] | 0.95[a] | 0.86[a] | 0.79[a] | 0.97[b] |
| | $m_r$ | 0.93 | 1.3 | 1.1 | 1.1 | 0.65 | 0.65 | 0.32 | 0.54 | 0.76 | 0.81 | 0.65 | 0.58 |
| | $b_r$ | −11 | −15 | −13 | −13 | −9.0 | −9.4 | −5.7 | −8.8 | −10 | −11 | −9.0 | −8.8 |
| B | $r^2$ | 0.92[a] | 0.92[a] | 0.88[a] | 0.96[a] | 0.78[a] | 0.61[a] | 0.85[a] | 0.74[a] | 0.96[a] | 0.62[b] | 0.88[a] | 0.83[a] |
| | $m_r$ | 1.1 | 1.0 | 0.91 | 1.1 | 0.57 | 0.19 | 0.41 | 0.40 | 0.89 | 0.56 | 0.77 | 0.67 |
| | $b_r$ | −13 | −13 | −12 | −13 | −8.1 | −4.2 | −6.6 | −6.5 | −12 | −7.8 | −10 | −9.2 |
| C | $r^2$ | 0.87[a] | 0.90[a] | 0.94[a] | 0.89[a] | 0.94[a] | 0.55[a] | 0.80[a] | 0.52[b] | 0.97[a] | 0.75[a] | 0.95[a] | 0.87[a] |
| | $m_r$ | 0.71 | 0.89 | 0.99 | 0.92 | 0.74 | 0.20 | 0.42 | 0.35 | 0.84 | 0.72 | 0.90 | 0.71 |
| | $b_r$ | −9.2 | −11 | −12 | −12 | −10 | −4.7 | −6.8 | −6.3 | −11 | −9.4 | −11 | −10 |

[a] Significant at $P \leq 0.01$. [b] Significant at $P \leq 0.05$.

by 10% om content for the particles. PAHs were in general near the partitioning curve predicted for 10−20% om content.

Correlation results for log $K_p$ versus log $K_{oa}$ are shown in Table 4 and were in general highly significant (at $P \leq 0.01$) for PCDD/Fs, PCBs, and PAHs. Figure 3 shows log $K_p$-log $K_{oa}$ plots for site A (those for sites B and C are available as Figures 1S and 2S in the Supporting Information).

**Comparison of $p_L$ and $K_{oa}$ as Descriptors of Partitioning**. It is important to note that both $p_L$ and $K_{oa}$ are excellent descriptors of gas-particle partitioning for PCBs, PAHs, and PCDD/Fs. Regression coefficients were similar for PCBs and PAHs, while regression coefficients for PCDD/Fs were in general higher using $p_L$ but still highly significant for log $K_p$-log $K_{oa}$ regressions (see Tables 3 and 4). This shows that $p_L$ is a valid descriptor of both ad- and absorption processes. The higher regression coefficients using $p_L$ may indicate a significant adsorptive contribution for low organic matter aerosols for which $p_L$ is a valid descriptor but not necessarily $K_{oa}$.

Based on the $K_{oa}$ absorption model (eq 5) it is possible to calculate $f_{om}$ in the aerosols, as measured by the partitioning data. The mean PCDD/F-intercepts from sites A to C correspond to a $f_{om}$ of 4% (site A), 20% (B), and ∼100% (C) in the aerosol (see eq 5). A higher $f_{om}$ can be expected for the predominantly low-temperature aerosols (associated with wood burning) at the rural sites (*40*). Site C was further characterized by consistently high PAH concentrations (*21*), which could partially explain the too high $f_{om}$ estimation based on the $K_{oa}$-model. Interestingly, higher regression coefficients for PCDD/Fs were obtained for the sites characterized by a low $f_{om}$, namely sites A ($p_L$-$r^2$: 0.94; $K_{oa}$-$r^2$: 0.89) and B ($p_L$-$r^2$: 0.93; $K_{oa}$-$r^2$: 0.87). Hence, *ad*sorption could explain the difference of the two models with better log $K_p$-log $p_L$ regression coefficients.

$K_{oa}$-PCDD/F regression lines were steepest and most were near +1; most $K_{oa}$-PAH regression slopes were ∼0.7 to 0.8 but not significantly different from +1, whereas $K_{oa}$-PCBs showed the shallowest slopes (∼0.3 to 0.7) and were significantly different from +1. $p_L$-PCDD/Fs regression lines were steepest and often significantly different from −1; most $p_L$-PAH regression slopes were ∼ −0.6 to −0.8 and significantly different from −1, whereas $p_L$-PCBs showed the shallowest slopes, ∼ −0.3 to −0.7, and were significantly different from −1. Both models, hence, show similar relative states of gas-particle partitioning for PAHs, PCBs, and PCDD/Fs. We will now explore if there are any site or event differences apparent for PAHs, PCBs, and PCDD/Fs.

**Comparison of Sites**. Both models agree that PAHs were closest to equilibrium at site C: for $p_L$-regressions PAH-slopes were closest to −1 (mean −0.8) at site C and ∼ −0.7 at sites A and B. Similarly, for the $K_{oa}$-model, PAH $m_r$-values were closest to +1 at site C (mean 0.8) and ∼0.7 at sites A and B. All sites considered in this study had strong local inputs of PAHs, namely traffic, industry, and housing at urban site A and domestic burning at rural sites B and C. Slopes more shallow than −1 have been observed for PAHs sampled in urban/source regions before (e.g. refs *18* and *19*). In Chicago ($p_L$-) slopes were on average −0.64 and −0.69 for PAHs (*18*, *19*). This compares well to slopes derived in this study of −0.71 for PAHs. Slower absorption from the gas phase of the heavier members of PAHs to combustion aerosols as they cool and age may account for the shallow slopes (*19*). A similar reasoning can explain the states of equilibrium at the rural sites, being strongly influenced by local domestic burning of coal and wood. Ambient concentrations of PAHs at the rural sites B and C were quite similar to those at the urban site A. Locally released PAHs need to equilibrate to the ambient temperature and background particles present, which can

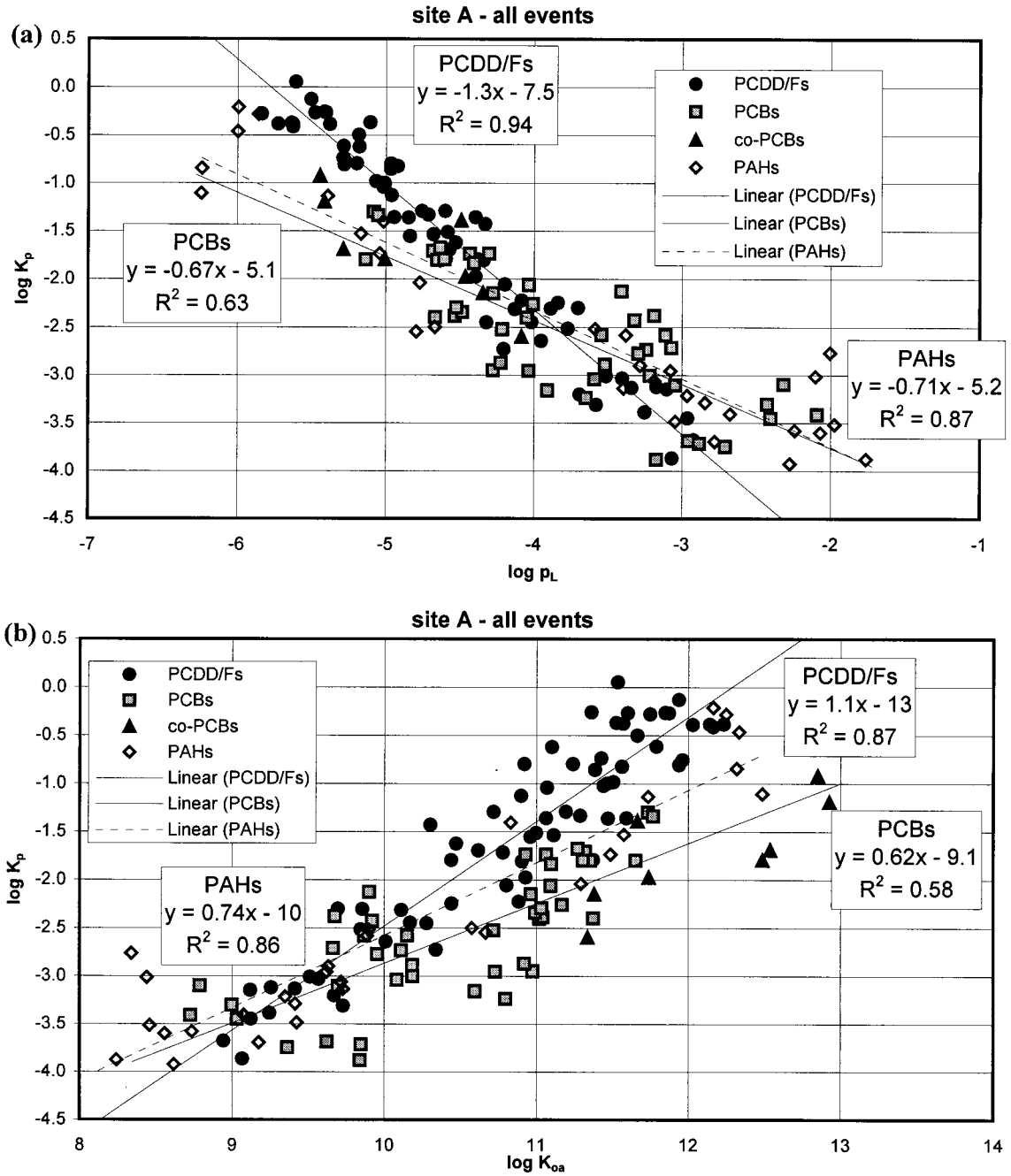


**FIGURE 3. (a) Log $K_p$-log $p_L$ and (b) log $K_p$-log $K_{oa}$ plots for all events at site A.**

result in slopes more shallow than −1 (see also Figure 3 and Figures 1S and 2S in the Supporting Information).

The $p_L$ and the $K_{oa}$ model show similar trendlines for PCBs; in both models site A was closest to equilibrium: $p_L$-$m_r$-values for PCBs at site A were closest to −1 (mean −0.64) but only ∼−0.5 at the other sites. $K_{oa}$-$m_r$-values for PCBs were closest to +1 at site A (mean 0.58) but only ∼0.4 at the other sites. Studies of PCBs in urban locations found slopes more shallow than −1 (e.g. refs *18* and *19*). In Chicago ($p_L$-) slopes were on average −0.73 and −0.51 for PCBs (*18, 19*), similar to a $p_L$-PCB slope of −0.64 in this study. We hypothesize that the shallow slopes for PCBs at the rural sites is due to slow reequilibrium of advected PCBs to freshly emitted particulate matter. This hypothesis is outlined graphically in Figure 4a.

As already discussed, the rural sites were not significant sources of PCBs (*35*) which were mostly introduced by advective transport and will have already approached gas-particle equilibrium (see line 1 in Figure 4a). However, the rural sites released particulate matter (containing relatively low quantities of PCBs) from domestic burning, which offset the established gas-particle equilibrium (line 2 in Figure 4a). Initially, this will result in a lower value for $K_P$ (see eq 3) and thus reduce the intercept value in log $K_p$-log $p_L$/log $K_{oa}$ plots. Consecutively, the more volatile PCBs will reequilibrate faster and thus alter the slope of the log $K_p$-log $p_L$/log $K_{oa}$ plots. This rapid redistribution of the more volatile PCBs to the new particulate matter will result in slopes more shallow than −1 ($p_L$) or +1 ($K_{oa}$) (see line 3 in Figure 4a). This may explain why for PCBs we observed slopes that were much shallower than unity at the rural sites B and C (e.g. see Figure 3 and Figures 1S and 2S in the Supporting Information).

So far, $p_L$- and $K_{oa}$-based regressions agreed on the states of equilibrium for PAHs and PCBs at the different sites. Concerning PCDD/Fs, the $p_L$-model showed mean slopes at

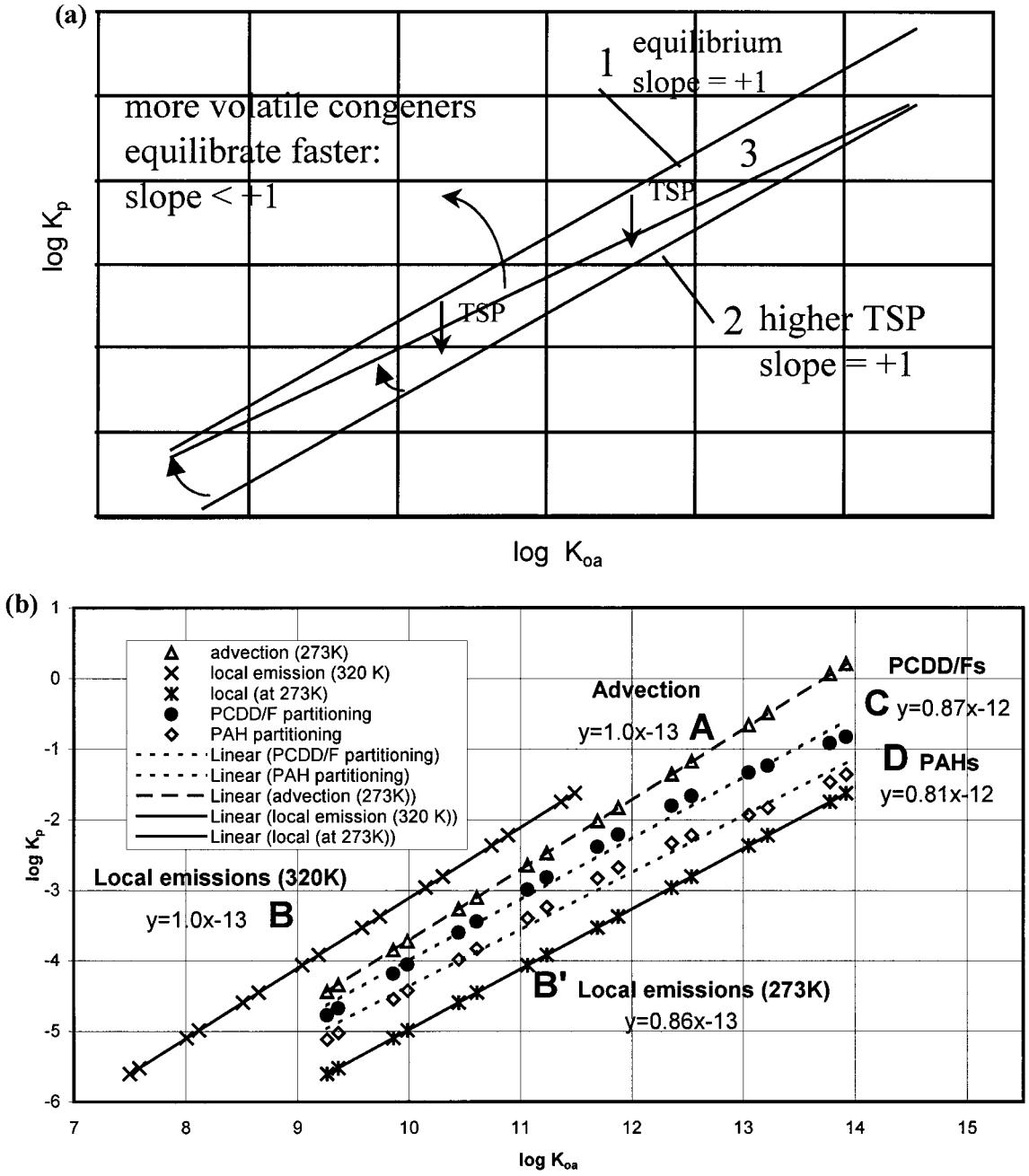


**FIGURE 4. Schematic diagrams of (a) changes in TSP and (b) the relative importance of advection and local emissions affecting slope and intercept of gas-particle distributions.**

sites A (−1.3) and B (−1.2) being significantly (at $P \leq 0.05$) different from −1, whereas PCDD/F partitioning at site C ($m_r = -1.1$) was suggestive of equilibrium in the samples. However, in the $K_{oa}$-model PCDD/Fs-regression slopes were ∼+1. Only two of the 12 PCDD/F regressions were significantly different (at $P \leq 0.05$) from equilibrium partitioning ($m_r = +1$), namely (site) A − (event) II and C−I. There was a significant (at $P \leq 0.05$) difference between PCDD/Fs at sites A and C, with the average $m_r$ (A) > $m_r$ (C). Similarly, there was a significant difference between the intercepts at both sites, with $b_r = -13.3$ (site A) significantly (at $P \leq 0.05$) higher than $b_r = -11.2$ (C) with $b_r = -12.6$ (B) (see also Figure 3 and Figures 1S and 2S in the Supporting Information).

In summary, $p_L$ described PCDD/Fs at sites A and B not being in equilibrium, with PCDD/Fs at site C having reached equilibrium, while the correlations with $K_{oa}$ showed the opposite, i.e., PCDD/Fs at sites A and B were generally in gas-particle equilibrium but not at site C. Both models agreed, however, on the relative states of equilibrium of PCBs and PAHs. *Nevertheless, there was no consistent difference between the urban and the rural sites apparent.*

We will now explore if events had a stronger impact on the partitioning.

**Comparison of Events.** Event I was characterized by the coldest $T$ (<0 °C), high TSP-concentrations and the highest ambient air concentrations of PAHs and PCDD/Fs. Event IV, on the contrary, was characterized by the warmest $T$ and in general by the highest PCB and lowest PAH and PCDD/F concentrations. There was no significant difference between the partitioning of PAHs at the four events apparent in either model (at $P \leq 0.05$). Regression slopes were steepest on event I ($K_{oa}$: 0.83; $p_L$: −0.77) and shallowest on event IV ($K_{oa}$: 0.70; $p_L$: −0.67). The $K_{oa}$ and the $p_L$ model showed a significant difference (at $P \leq 0.05$) between event I and events II and III, with PCB-regression slopes steeper for event I ($K_{oa}$: 0.63;

$p_L$: −0.71) than for events II and III ($K_{oa}$: 0.36, 0.38; $p_L$: −0.45, −0.42).

In the $K_{oa}$-model for PCDD/Fs event I had the shallowest slope (0.87), which was significantly different from +1 (at $P \leq 0.05$); but there were no other significant difference between the events. By contrast the $p_L$-model showed PCDD/Fs only for event I not being significantly different from a slope of −1 ($m_r = -1.07$), whereas for the other events the slopes were significantly different (at $P \leq 0.05$).

For event I, when favorable meteorological conditions (i.e. low ambient $T$ and wind speed) increased PAH and PCDD/F-concentrations by factors of 2−4, the partitioning of PAHs and PCDD/Fs was similar: $K_{oa}$-regression slopes were 0.83 (PAHs) and 0.87 (PCDD/Fs) and significantly different from +1. Cold ambient temperatures may have slowed the exchange between the gaseous and particulate fraction. An important difference between ambient PAHs and PCDD/Fs was the relative importance of regional versus local emissions. Local emission accounted for ∼75% of ΣPAHs at rural sites B and C but only for 25% of PCDD/Fs (*21*). Clearly, local emissions will not have reached equilibrium while "aged", regional background concentrations had more time to partition between the gaseous and particulate phase. A simple model illustrates this in Figure 4(b): the two "ideal" partitioning lines represent POPs arriving by advective transport (line A: at 273 K, $f_{om}$ 0.05, TSP 30 $\mu g/m^3$) and local emissions (line B: at 320 K, $f_{om}$ 0.20, TSP 60 $\mu g/m^3$). PCDD/Fs and PAHs are assumed to be in gas-particle equilibrium at their respective $T$. For PCDD/Fs, we assumed 75% advective transport and 25% local emissions; for PAHs 25% advective transport and 75% local emissions. At the rural sites, the locally released TSP, PAH, and PCDD/F emissions mix with those arriving by advective transport. The resulting partitioning lines assume that the mixed PCDD/Fs and PAHs have not yet reached equilibrium between the warm, local emissions and the cold, advective ambient air masses: for PAHs, the locally released 75% still reflect the partitioning at 320 K, i.e. a higher proportion in the gaseous phase than the "advective" PAHs at 273 K. Line B′ depicts the partitioning of these locally released PAHs at the ambient $T$ of 273 K which results in a slope <1. In that case, slopes shallower than +1 result for PCDD/Fs (line C: +0.87) and PAHs (line D: +0.81). A combination of advection and local releases during cold ambient $T$ could explain why PCDD/Fs were closer to equilibrium than PAHs, which were predominantly locally released. For the following, warmer events, steeper regression slopes were observed for PCDD/Fs, in line with $T$ being the main reason for the disequilibrium. Indeed, Kamens et al. (*16*) observed that at $T$ below 0 °C, tens of hours are required for PAHs such as Phen and Pyr to reestablish equilibrium. Similarly, a study of PCDD/F partitioning in northern England found PCDD/Fs to deviate from gas-particle equilibrium partitioning only during sampling events with $T$ of ∼0 °C (*41*).

In summary, then, the $K_{oa}$ model and the $p_L$ model were used to describe gas-particle partitioning of PCDD/Fs, PCBs, and PAHs. Both the $K_{oa}$ model and the $p_L$ model showed a different partitioning behavior for PAHs, PCBs, and PCDD/Fs. Whereas PCBs and PAHs showed deviations from equilibrium partitioning, PCDD/Fs in general met the criteria of equilibrium partitioning (slope near 1). In the case of PAHs, local releases at all three sites can explain the lack of equilibrium partitioning. PCBs did not show equilibrium partitioning at any site, but were closest to equilibrium partitioning during the coldest sampling event. It is argued that the locally released aerosols at the rural sites disturbed their partitioning. $p_L$- and $K_{oa}$-based regressions showed different states of equilibrium for PCDD/Fs at the sites. A simple $K_{oa}$-model showed PAHs and PCDD/Fs not being in equilibrium for event I, in line with expectations based on the relative importance of advection and local releases at those sites.

It seems appropriate to mention certain limitations of this study which should be addressed in further gas-particle research: (i) the need of additional information on the aerosol properties (e.g. their om content) [It would have greatly strengthened the conclusions tentatively drawn in this study.]; (ii) the lack of physical-chemical properties of PAHs [There are no consistent and comprehensive data for PAH-$p_L$ and only a very limited study of their $K_{oa}$-values.]; (iii) the most sensitive variable in describing the gas-particle partitioning is $T$ [Minimizing the $T$-fluctuation by means of short sampling periods and/or a constant monitoring of $T$ at the sampling site is desirable.]; and (iv) the selection of a further sampling site downwind of emission sources would be helpful in testing the reasons for disequilibrium of gas-particle partitioning outlined in this study.

## Acknowledgments

We thank the landlords of the "New Inn" in Clapham and the "Game Cock" in Austwick for their courtesy of offering us sampling sites. We thank Dr. Robert Lee for his help in the setting up and operation of the sites, Dr. Mike Howsam, Dr. Grant Northcott, and Dr. Nicholas Green for analytical help and Dr. Mick Green for advise on statistical matters. We are grateful to DETR and MAFF for financial support for POPs research.

## Supporting Information Available

Figures 1S and 2S of log $K_p$-log $p_L$ and log $K_p$-log $K_{oa}$ plots for sites B and C. This material is available free of charge via the Internet at http://pubs.acs.org.

## Literature Cited

(1) Bidleman, T. F. *Environ. Sci. Technol.* **1988**, *22*, 361−367.
(2) Pankow, J. F.; Bidleman, T. F. *Atmos. Environ.* **1991**, *25A*, 2241−2249.
(3) Pankow, J. F. *Atmos. Environ.* **1994**, *28*, 185−188.
(4) Pankow, J. F.; Bidleman, T. F. *Atmos. Environ.* **1992**, *26A*, 1071−1080.
(5) Finizio, A.; Mackay, D.; Bidleman, T.; Harner, T. *Atmos. Environ.* **1997**, *31*, 2289−2296.
(6) Harner, T.; Bidleman, T. F. *Environ. Sci. Technol.* **1998**, *32*, 1494−1502.
(7) Pankow, J. F. *Atmos. Environ.* **1998**, *32*, 1493−1497.
(8) Kaupp, H.; McLachlan, M. S. *Chemosphere* **1999**, *38*, 3411−3421.
(9) Goss, K.-W.; Schwarzenbach, R. P. *Environ. Sci. Technol.* **1998**, *32*, 2025−2032.
(10) Harner, T.; Mackay, D. *Environ. Sci. Technol.* **1995**, *29*, 1599−1606.
(11) Harner, T.; Bidleman, T. F. *J. Chem. Eng. Data* **1996**, *41*, 895−899.
(12) Kömp, P.; McLachlan, M. S. *Environ. Tox. Chem.* **1997**, *16*, 2433−2437.
(13) Harner, T.; Bidleman, T. F. *J. Chem. Eng. Data* **1998**, *43*, 40−46.
(14) Harner, T.; Green, N.; Jones, K. C. *Environ. Sci. Technol.* **2000**, *34*, 3109−3114.
(15) Harner, T.; Mackay, D.: Jones, K. C. *Environ. Sci. Technol.* **1995**, *29*, 1200−1209.
(16) Kamens, R.; Odum, J.; Fan, Z.-H. *Environ. Sci. Technol.* **1995**, *29*, 43−50.
(17) Pennise, D. M.; Kamens, R. *Environ. Sci. Technol.* **1996**, *30*, 2832−2842.
(18) Simcik, M. F.; Franz, T. P.; Zhang, H.; Eisenreich, S. J. *Environ. Sci. Technol.* **1998**, *32*, 251−257.
(19) Cotham, W. E.; Bidleman, T. F. *Environ. Sci. Technol.* **1995**, *29*, 2782−2789.
(20) Kaupp, H.; McLachlan, M. *Chemosphere* **1999**, *38*, 3411−3421.
(21) Lohmann, R.; Northcott, G. L.; Jones, K. C. *Environ. Sci. Technol.* **2000**, *34*, 2892−2899.
(22) Lohmann, R.; Green, N. J. L.; Jones, K. C. *Environ. Sci. Technol.* **1999**, *33*, 2872−2878.
(23) Thomas, G. O.; Sweetman, A. J.; Parker, C. A.; Kreibich, J.; Jones, K. C. *Chemosphere* **1998**, *36*, 11, 2447−2459.

(24) Howsam, M.; Ineson, P.; Jones, K. C. *Water, Air, Soil Pollut.* **2000**, *121*, 379−398.
(25) Lee, R. G. M.; Jones, K. C. *Environ. Sci. Technol.* **1999**, *33*, 3596−3604.
(26) Eitzer, B. D.; Hites, R. A. *Environ. Sci. Technol.* **1988**, *22*, 1362−1364. Addition/Correction *Environ. Sci. Technol.* **1998**, *32*, 2804.
(27) Donelly, J. R.; Munslow, W. D.; Mitchum, R. K.; Sovocool, G. W. *J. Chromatogr.* **1987**, *392*, 51−63.
(28) Hale, M. D.; Hileman, F. D.; Mazer, T.; Shell, T. L.; Noble, R. W.; Brooks, J. J. *Anal. Chem.* **1985**, *57*, 640−648.
(29) Yamasaki, H.; Kuwata, K.; Kuge, Y. *Nippon Kagaku Kaishi* **1984**, *8*, 1324−1329 (in Japanese); *Chem. Abstr. 101*, p 156747.
(30) Falconer, R. L.; Bidleman, T. F. *Atmos. Environ.* **1994**, *28*, 547−554.
(31) Mackay, D.; Shiu, W. Y.; Ma, K. C. *Illustrated handbook of physical-chemical properties and environmental fate for organic chemicals Vol. II PAHs, PCDD/Fs*; Lewis Publishers: 1991; ISBN 0-87371-513-6.
(32) Lohmann, R.; Jones, K. C. *Sci. Tot. Environ.* **1998**, *219*, 53−81.
(33) Halsall, C. J.; Lee, R. G. M.; Coleman, P. J.; Burnett, V., Harding-Jones, P.; Jones, K. C. *Environ. Sci. Technol.* **1995**, *29*, 2368−2376.
(34) Halsall, C. J.; Coleman, P. J.; Davis, B. J.; Burnett, V., Waterhouse, K. S.; Harding-Jones, P.; Jones, K. C. *Environ. Sci. Technol.* **1994**, *28*, 2380−2386.
(35) Coleman, P. J.; Lee, R. G. M.; Alcock, R. E.; Jones, K. C. *Environ. Sci. Technol.* **1997**, *31*, 2120−2124.
(36) Van den Berg, M.; Birnbaum, L.; Bosveld, A. T. C.; Brunström, B.; Cook, P.; Feeley, M.; Gisey, P.; Hanberg, A.; Hasegawa, R.; Kennedy, S. W.; Kubiak, T.; Larsen, J. C.; van Leeuwen, R. F. X.; Liem, A. K. D.; Nolt, C.; Peterson, R. E.; Poellinger, L.; Safe, S.; Schrenk, D.; Tillit, D.; Tysklind, M.; Younes, M.; Waern, F.; Zacharewski, T. *Environ. Health Persp.* **1998**, *106*, 775−792.
(37) Junge, C. E. In *Fate of Pollutants in the Air and Water Environment*; Suffet, I. H., Ed.; Wiley-Interscience: New York, 1977; Part 1, Vol. 8, p 7-5.
(38) Pankow, J. F. *Atmos. Environ.* **1987**, *22*, 2275−2283.
(39) Yamasaki, H.; Kuwata, K.; Miyamato, H. *Environ. Sci. Technol.* **1982**, *16*, 189−194.
(40) Simo, R.; Grimalt, J. O.; Albaiges, J. *Environ. Sci. Technol.* **1997**, *31*, 2697−2700.
(41) Lohmann, R.; Lee, R. G. M.; Green, N. J. L.; Jones, K. C. *Atmos. Environ.* **2000**, *34*, 2529−2537.

*Received for review November 30, 1999. Revised manuscript received May 8, 2000. Accepted September 1, 2000.*

ES9913232